Layered liquid-liquid flow in microchannels having selectively modified hydrophilic and hydrophobic walls

Yoshikazu Yamasaki*, Masato Goto*, Akira Kariyasaki*, Shigeharu Morooka*,†,
Yoshiko Yamaguchi**, Masaya Miyazaki**,***, and Hideaki Maeda**,***

*Department of Chemical Engineering, Fukuoka University, Fukuoka 814-0180, Japan
**Nanotechnology Research Institute, National Institute of Advanced Industrial Science and Technology (AIST),
Tosu 841-0052, Japan
***Department of Molecular and Material Sciences, Interdisciplinary Graduate School of Engineering Sciences,
Kyushu University, Kasuga 816-8580, Japan

Abstract−When two immiscible liquids make contact in a microchannel, the flow pattern is affected by the affinity between channel walls and liquids. In this study, microchannels (200 µm in width and 200 µm in depth) having a T-shaped bifurcation point were fabricated on PMMA plates. The inner walls of the microchannels were modified in a zone-selective manner to be either hydrophilic or hydrophobic, based on verification accomplished via a laser interference fringe technique. The microchannel was placed horizontally, and water and octane were introduced into the upper-side channel (hydrophilic) and into the lower-side channel (hydrophobic), respectively. The experimental results showed that water and octane formed a stable layered flow, and the two liquids were virtually completely separated at the T-shaped section, even when static pressure was intentionally applied to the outlets. CFD simulation, using FLUENT 6.3 software, was performed to explain the role of zone-selective modification of microchannel walls.

Key words: Microchannel, Layered Flow, Wettability, Surface Modification, CFD Simulation

INTRODUCTION

For liquid-phase systems, the diffusion rate is an important factor in controlling reaction rates. In microchannels, the surface area per unit volume is large in comparison with conventional reactors, and such characteristics provide a variety of applications in chemical processing and analytical fields [1-7]. Since different flow patterns are possible for liquid-liquid systems [8], the design of a microchannel contactor requires that the flow pattern be controlled such that it will be suitable for a particular purpose. We investigated the fluidic behavior for miscible liquid phases in a microchannel by observing flow patterns, and by using computational fluid dynamics (CFD) simulation [9,10].

The two-phase flows of immiscible liquids with a large interfacial tension, such as in the case of water and octane, are different from the flows of miscible liquids. In microchannels, capillary number, which describes the contribution of the interfacial tension by comparing viscous force, is much less than unity. This suggests that flow patterns of immiscible liquids in a microchannel are strongly dependent on the affinity between the liquids and the inner solid walls of the microchannel. In a material extraction system where immiscible water/oil laminar flow is applied, two flow patterns are possible: dispersed flow and layered flow [11]. The latter is sometimes preferable because it does not require the separation of droplets. Approaches directed toward a liquid-liquid layered flow have been reported; a notable example includes modifying microchannel inner walls into hydrophilic and hydrophobic surfaces [12-15]. In

some cases, however, the orientation of the two-phase liquid layered flow has been side-by-side in a horizontal microchannel. To realize a stable layered flow of any orientation, control of the wettability of microchannel inner walls is a necessity.

In the present study, we fabricated sealed microchannels, the inner walls of which were modified zone-selectively to be both hydrophilic and hydrophobic. We also evaluated the hydrophilicity and hydrophobicity of the solid surfaces by determining contact angles from interference fringe patterns. Water and octane were then introduced into the microchannel, which was placed in a horizontal position (upper-hydrophilic channel; and lower-hydrophobic channel), and separated at a T-shaped bifurcation point, and discharged to the outside. The effects of the zone-selective modification of channel walls and the interfacial tension on the separation of liquids were evaluated by CFD simulation using FLUENT 6.3 software.

EXPERIMENTS AND RESULTS

1. Fabrication of Microchannels and Zone-selective Surface Modification

Microchannels (width=200 µm, depth=100 µm, straight path length=40 mm), Fig. 1(a), were fabricated mechanically on PMMA plates by using an NC lathe (PMT Co., Japan) and a flat-end mill that was 200 µm in diameter. The flat surface, other than the incised microchannel, was masked, and an Au thin film was formed by sputtering on only the inner walls of the microchannel. Also, a hydrophilic microchannel was prepared by coating the inner walls with a TiO$_2$-based coating agent (#ENS245, TOTO Co., Japan). The microchannels were then joined face to face, as shown in Fig. 1(b), and were seal-bonded under pressure and elevated temperature in

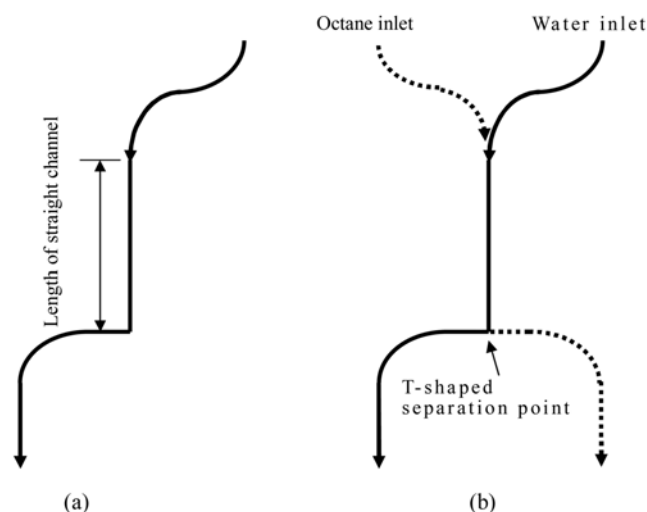†To whom correspondence should be addressed.
E-mail: smorooka@fukuoka-u.ac.jp

Fig. 1. Microchannel with a T-shaped separation point. (a) Microchannel pattern, (b) flow scheme in bonded microchannel.

a vacuum oven (as a result, the depth became 200 μm). Fig. 2(a) shows the dimensions of the major part of the microchannel. After bonding, inlet and outlet tubing was connected. Then, an ethanol solution of 1 mmol L⁻¹ 1-octadecanethiol was introduced into the microchannel with a fluid velocity of 1 μL min⁻¹ for 12 hours. To enhance the hydrophilicity of the TiO_2 layer, the microchannel was irradiated by UV light. Using this procedure, the inner walls of one-half of the microchannel were modified to be hydrophilic, while those of the other half of the microchannel were hydrophobic, as shown in Fig. 2(b). For comparison, a microchannel of the same dimensions, as shown in Fig. 2(a), was prepared with no surface modifications.

2. Chemicals Used and Physical Properties

Water (pure water grade, Wako Pure Chemicals, Japan) and octane (special reagent grade, Wako Pure Chemicals, Japan) were used,
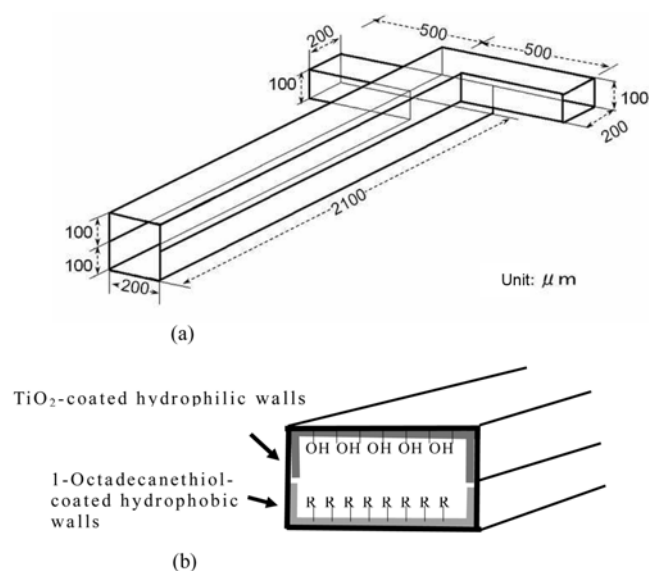

Fig. 2. Details of microchannel. (a) Major part dimensions (numerals are in units of μm), (b) modification model.
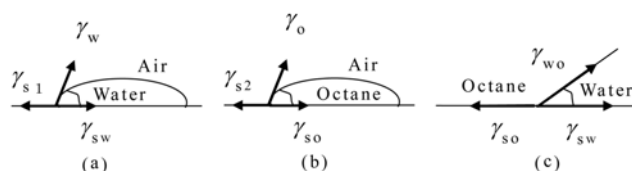
Fig. 3. Equilibria of surface forces. (a) Water drop on surface placed in air, (b) octane drop on surface placed in air, and (c) water drop on hydrophilic surface immersed in octane.

after the solubility equilibrium was attained at 298 K. The properties of pure components were used because of the scarce mutual solubility.

Water: density 998 kg m⁻³, viscosity 1.03 mPa s, surface tension 0.0719 N m⁻¹, refractive index 1.33

Octane: density 720 kg m⁻³, viscosity 0.54 mPa s, surface tension 0.0212 N m⁻¹, refractive index 1.20

The interfacial tension between water and octane was determined by using the conventional Du Nouy's method with a Pt ring, and was found to be equal to the calculated difference of the two liquids.

3. Contact Angles on Modified Surfaces

The affinity between the liquids and the solid surfaces is decided by a combination of the surface tension and the contact angle on the surface. Figs. 3(a), (b) and (c) show the surface forces acting on a water drop placed on a hydrophilic surface in ambient air, on an octane drop placed on a hydrophobic surface in ambient air, and on a water drop surrounded by octane on a hydrophilic surface, respectively. The balance among the surface forces is described as

$$\gamma_{s1} = \gamma_w \cos\alpha_w + \gamma_{sw} \tag{1}$$

$$\gamma_{s2} = \gamma_o \cos\alpha_o + \gamma_{so} \tag{2}$$

$$\gamma_{so} = \gamma_{wo} \cos\alpha_{wo} + \gamma_{sw} \tag{3}$$

If γ_{s1} is equal to γ_{s2}, the contact angle of water in the case where water and octane coexist, α_{wo}, is calculated from Eqs. (1)-(3) as follows:

$$\cos\alpha_{wo} = \frac{\gamma_w \cos\alpha_w - \gamma_o \cos\alpha_o}{\gamma_{wo}} \tag{4}$$

The surface that was modified to be hydrophilic by using the TiO_2 coating agent was porous, and the contact angle of octane on the surface was smaller than that of water. Therefore, γ_{s1} is not always equal to γ_{s2}. This suggests that the contact angle of a liquid phase surrounded by another liquid phase cannot be calculated from the contact angles that have been determined on the solid surface in ambient air.

The effect of the surface treatments on the improvement of liquid-solid affinity was evaluated with PMMA flat plates, which were modified by the identical procedures that were used for the microchannels. The combinations of liquids and solids in the present study were as follows.

Case 1: an octane drop on a TiO_2-coated surface that has been dipped in water

Case 2: a water drop on a TiO_2-coated surface that has been dipped in octane

Case 3: an octane drop on an octadecanethiol-modified surface that has been dipped in water
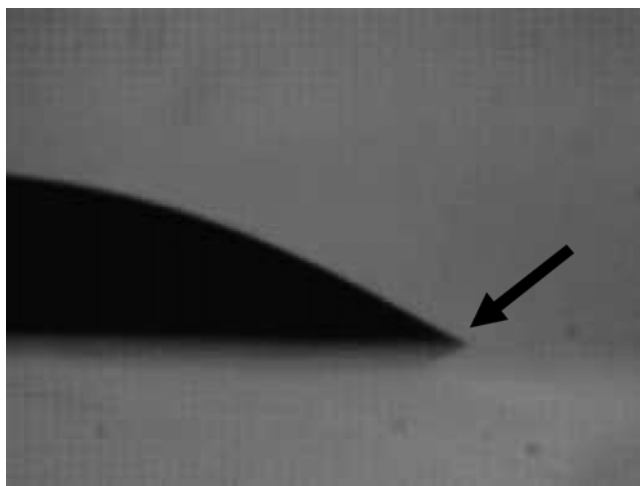
Fig. 4. Water drop on hydrophilic surface immersed in octane.

Case 4: a water drop on an octadecanethiol-modified surface that has been dipped in octane

The contact angles of the drops for Cases 1-4 were observed with a side view microscope. The octane drop did not stay attached to the TiO_2-coated surface that had been dipped in water (Case 1), although octane as a single phase in air showed a high affinity for the TiO_2-coated surface. The water drop on the octadecanethiol-modified surface that had been dipped in octane (Case 4) was nearly spherical. Thus, the coexistence of water and octane played an important role on the contact angle between the liquid and the solid surface.

Fig. 4 shows a side-view image of a water drop on a TiO_2-coated surface that has been dipped in octane (Case 2). The water drop was basically in a spherical-cap shape, but it is obvious that the fringe was extended in a thinner film. The octane drop on the octadecanethiol-modified surface that had been dipped in water (Case 3) showed a shape similar to the water drop in Case 2. Thus, the side-view photograph method was not amenable to precise determination of contact angles in Cases 2 and 3. We developed an interference fringe method for the measurement of small contact angles.

Fig. 5 shows the paths of laser light in a wedge-shaped liquid film. Although the thickness of an actual liquid drop is not uniform, we assumed, for the sake of simplicity, that the inclination
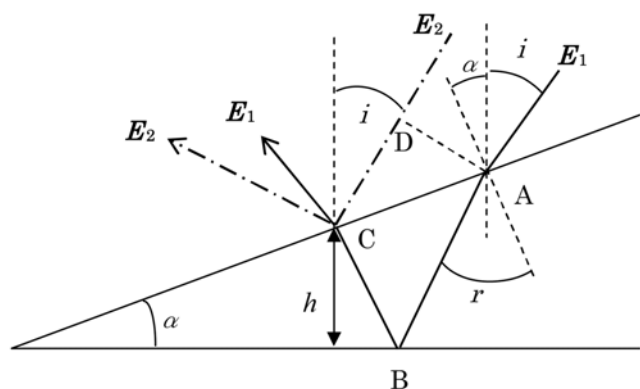
angle, α, was constant. Light E_1 appeared at point A at an angle i to the vertical line, refracted at point A and reflected at point B, then refracted again at point C. Complementary light E_2, which was coherent and parallel to light E_1, appeared at point C. Lights E_1 and E_2 were focused at point C on a CCD camera with a microscopic objective lens. Point D was the intersection of the perpendicular line drawn from point A to light E_2. The optical path length between lights E_1 and E_2 is given by $n_r(\overline{AB}+\overline{BC})-\overline{CD}$.

The refractive index is given by

$$n_r = \frac{\sin(\alpha+i)}{\sin r} \tag{5}$$

where $\alpha+i$ and r are the angles of the light to the line perpendicular to the inclined face. The optical path difference is given by

$$n_r(\overline{AB}+\overline{BC})-\overline{CD} = \frac{2n_r h}{1-\tan\alpha\tan(r-\alpha)}$$
$$\left[\frac{1}{\cos(r-\alpha)} - \frac{\sin(i+\alpha)\tan(r-\alpha)}{n_r\cos\alpha}\right] \tag{6}$$

where h is the liquid thickness at point C. The incremental height difference of the liquid layer between adjacent intensity extrema, Δh, is given by

$$\Delta h = \frac{\lambda h}{n_r(\overline{AB}+\overline{BC})-\overline{CD}} \tag{7}$$

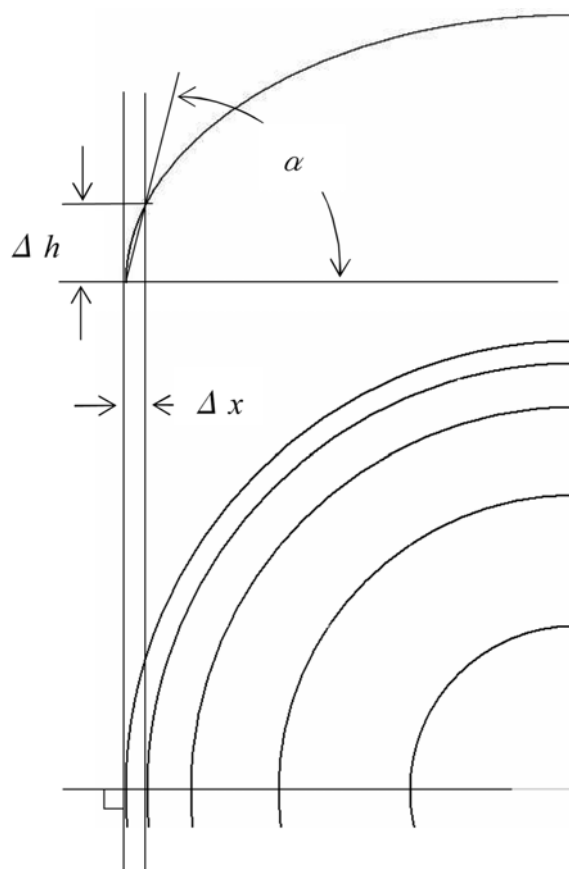By observing the distance between the neighboring interference

Fig. 6. Contours of fringes observed for a round drop: (a) side view, (b) top view.

Fig. 5. Relationship between incident and reflected rays.

extrema, the inclination angle is calculated from $\tan^{-1}(\Delta h/\Delta x)$. Fig. 6 schematically shows contours of fringes in the case of a spherical-cap drop.

When the inclination angle, α, is small, the optical path difference is approximated by $n_r(\overline{AB}+\overline{BC})-\overline{CD} \approx 2n_r h$, and the inclination angle is given by

$$\alpha \approx \tan^{-1}\left(\frac{\lambda}{2n_r\Delta x}\right) \tag{8}$$

Details of the interference fringe method were reported elsewhere [16]. A laser with $\lambda=543.5$ nm was used, and interferograms were
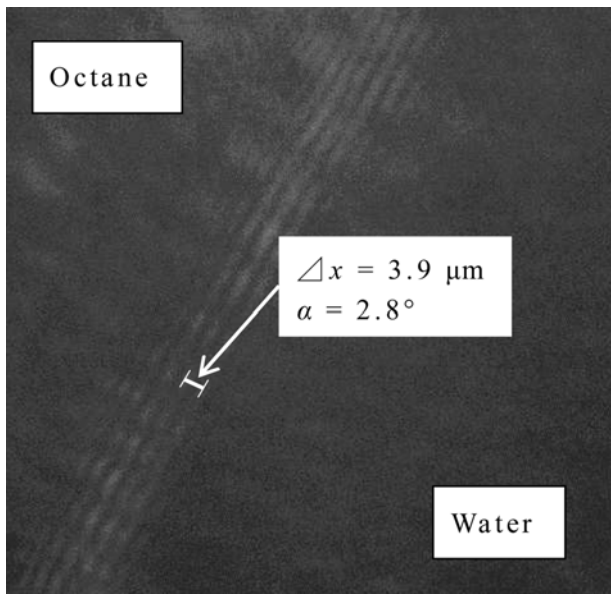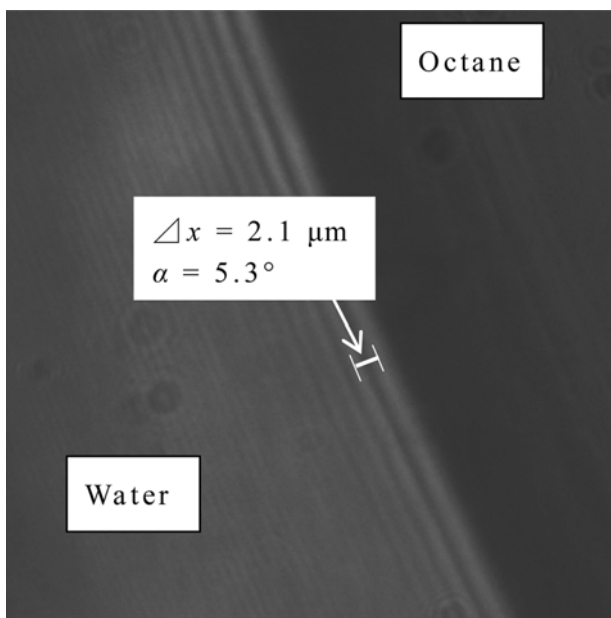
recorded with a 16-bit CCD video camera (SensiCam-670, pco. imaging, Germany). The distance between neighboring interference stripes, Δx, of the liquid drop was dependent on the location from the edge. In the present study, Δx was obtained by averaging the Δx values for the outmost 2-4 interference stripes.

Figs. 7 and 8 show the representative interferograms for a water drop on the TiO_2-coated surface dipped in octane (Case 2) and for an octane drop on the octadecanethiol-coated surface dipped in water (Case 3), respectively. The results show that the TiO_2-coated surface was sufficiently hydrophilic even when the surface was surrounded by octane, which alone formed a thin film on the TiO_2-coated surface in ambient air. In the coexisting octane, the contact angle of water was less than 7 degrees. Also, the octadecanethiol-modified surface was sufficiently hydrophobic. In coexisting water, the contact angle of octane was less than 5 degrees.

To ensure the effect of the surface treatment on the contact angle, a PMMA substrate was split into two sections: one part was hydrophilic (TiO_2-coated), and the other part was hydrophobic (octadecanethiol-coated). An octane drop placed on the substrate was dispersed on both sections. A water drop placed on the substrate, as shown in Fig. 9, was dispersed on the hydrophilic part, and stopped at the boundary between the hydrophilic and hydrophobic sections.

4. Stability of Two-phase Layered Flow

The microchannel was positioned horizontally. Water and octane were introduced into the upper-half and lower-half channels, respectively, as shown in Figs. 1 and 2. An orientation of the heavier water layer topside was purposely selected, because this scenario was more unstable than the reverse and required testing. The average flow velocity was kept at the same value, 0.8-4.0 cm s^{-1}, for each phase.

Fig. 7. Fringe pattern for octane film on the hydrophobic surface immersed in water ($\lambda=543.5$ nm).

Fig. 8. Fringe pattern for water film on the hydrophilic surface immersed in octane ($\lambda=543.5$ nm).
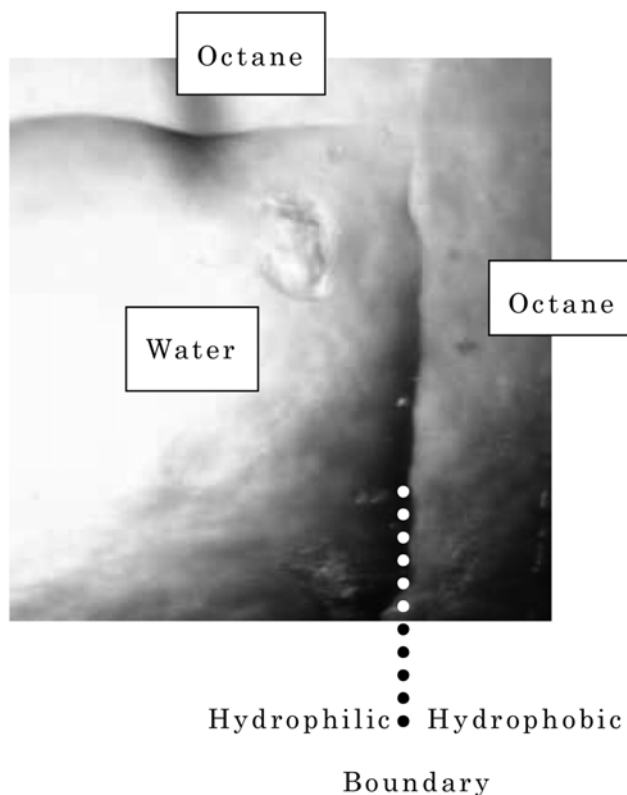

Fig. 9. Top view of zone-selectively modified surface.

The two-phase flow was divided at the T-shaped section into the upper and lower outlet flows. To decrease evaporation, the outlet flows were recovered in vials that contained anhydrous ethanol. The composition was analyzed by using a gas chromatograph (GC-8A, Shimadzu, Japan) with a hydrophobic separation column. The fraction of water in the hydrophilic upper-side outlet flow was calculated from

$$\frac{\text{Volume of recovered water}}{\text{Total volume of recovered liquids}} \qquad (9)$$

The fraction of octane in the hydrophobic lower-side outlet flow was calculated in a similar manner. Eq. (9) is meaningful only when the flow rate from the upper-side outlet is basically equal to that from the lower-side outlet. In the present study, the flow rates from the upper-side and lower-side outlets were coincident within 10%. Since water is more viscous than octane, a pressure loss in the water-side outlet tubing is possible to occur. Thus, the effect of the outlet pressure on the two-phase separation also was evaluated. The outlet pressure was applied by elevating one of the outlet tubing mouths.

The two-phase flow of water and octane in the microchannels with no zone-selective modification was found to be unstable and easily turned into a slug flow regime. Then, a mixture of water and octane was recovered evenly at the outlets. However, the two-phase layered flow in the microchannels, the walls of which were modified to be hydrophilic and hydrophobic, was quite stable. As shown in Fig. 10, the separation of water and octane was virtually complete.
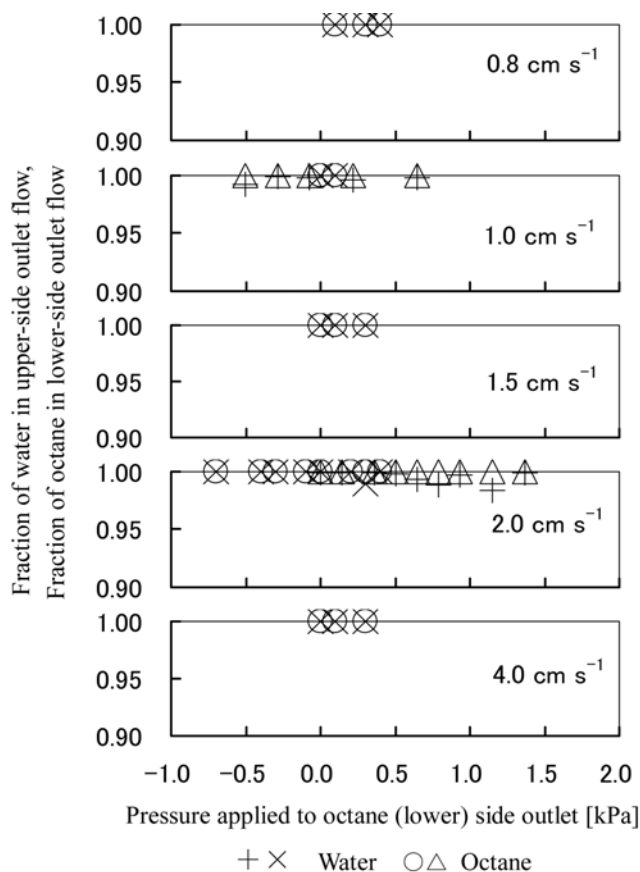

Fig. 10. Fractions of water and octane in upper- and lower-side outlet flows.

The pressure applied to one of the outlet mouths showed no practical impact on the separation within the values tested in the present study. A satisfactory separation was observed for the two microchannels prepared by the same procedures. This is shown by the different keys for each component in Fig. 10.

CFD SIMULATION OF TWO-PHASE FLOW

Three-dimensional simulation for two-phase flow in the microchannel was performed with a general-purpose computational fluid dynamics (CFD) package, FLUENT 6.3 (ANSYS, Inc.), based on a VOF model [9]. To evaluate the effect of the interfacial tension, a CSF model was used. Chemical reactions and interface mass transfer were not taken into account.

The experimental results described above indicate that the two-phase flow in microchannels was strongly affected by the contact angles of the water and the octane on the channel walls. At the T-shaped section, secondary flows (Dean vortex) may be formed in the water and octane layers by the centrifugal force, which is generated by the right-angle turn of the liquids. If the channel walls were not modified zone-selectively, the layered flow may have been turned into a slug flow, and no separation would be expected at the bifurcated outlets. Thus, the major purpose of the CFD simulation was to obtain a scheme for the effects of contact angles, and of pressures applied at the outlets, on the formation of a stable layered two-phase flow. The dimensions of the microchannel used in the CFD simulation were identical to the main part of the microchannels fabricated in this study (Fig. 2).

Assuming constant physical properties of water and octane, the unsteady-state equations of motion in the laminar region are given by the following equations.

For the water phase
$$\nabla \cdot \mathbf{v}_w = 0 \qquad (10)$$

$$\rho_w \frac{D\mathbf{v}_w}{Dt} = -\nabla p_w + \mu_w \nabla^2 \mathbf{v}_w + \rho_w \mathbf{g} \qquad (11)$$

For the octane phase
$$\nabla \cdot \mathbf{v}_o = 0 \qquad (12)$$

$$\rho_o \frac{D\mathbf{v}_o}{Dt} = -\nabla p_o + \mu_o \nabla^2 \mathbf{v}_o + \rho_o \mathbf{g} \qquad (13)$$

Static pressure and liquid velocity are distributed three-dimensionally in the microchannel. The boundary conditions on the walls are described by

$$\mathbf{v}_w = 0, \ \mathbf{v}_o = 0 \qquad (14)$$

The boundary conditions on the interface of water and octane are based on the assumption of no slip and on the momentum balance, and are given by the following equations.

$$\mathbf{v}_w = \mathbf{v}_o \qquad (15)$$

$$-\mu_w \frac{d\mathbf{v}_w}{d\mathbf{n}_i} = -\mu_o \frac{d\mathbf{v}_o}{d\mathbf{n}_i} \qquad (16)$$

where $\mathbf{n}_i$ is the unit vector vertical to contacting wall. Laplace's equation on the water and octane interface is given by the following equation.

$$\Delta p_{wo} = \gamma_{wo} \nabla \cdot \mathbf{n}_i \tag{17}$$

The curvature of the interface $\nabla \cdot \mathbf{n}_i$ varies depending on densities and viscosities of the fluids, as well as on the pressure applied to the outlet. This is distinct from the single-phase capillary phenomenon, where the contact angle is decided by the affinity between the liquid and the solid surface. When the microchannel walls are modified zone-selectively to be sufficiently hydrophilic and hydrophobic, both side edges of the interface for the two-phase layered flow are fixed on the peripheral lines between the tightly bonded upper and lower channels. However, a two-phase layered flow may turn into a slug flow, where the edges of the water-octane interface are no longer fixed on the peripheral lines of the upper and lower channels. In the present CFD simulation, therefore, contact angles for the coexisting water and octane system varied widely, and the flow patterns were calculated.

At the inlets, water and octane are introduced as single phases at velocities of $v_{w,in}$ and $v_{o,in}$, respectively.

$$\mathbf{v}_w = v_{w,in}, \ \mathbf{v}_o = v_{o,in} \tag{18}$$

At the outlets, constant pressure conditions are applied.

$$p_w = p_o = p_{u,out}, \ p_w = p_o = p_{1,out} \tag{19}$$

where $p_{u,out}$ and $p_{1,out}$ are the pressures of the upper and lower outlets.
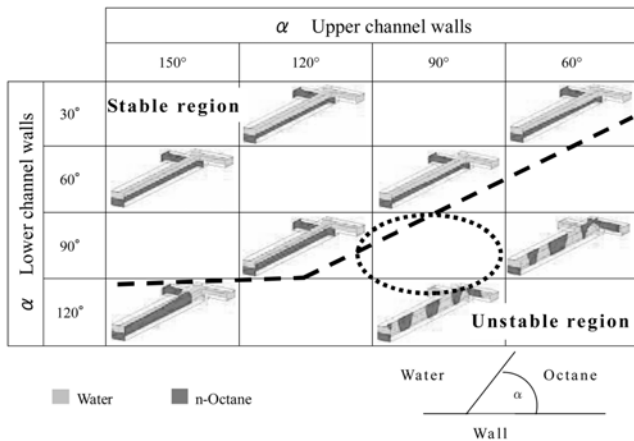

Fig. 11. CFD simulation for water (upper) and octane (lower) systems in microchannels with different contact angles. The broken line indicates an approximate boundary between the stable and unstable regions for the two-phase layered flow. The circled domain indicates the contact angles obtained with an untreated PMMA plate.

Meshes for computation were generated with GAMBIT 2.1 software. The details are reported elsewhere [15]. The mesh size was 5 μm×5 μm for the cross-sectional plane and 5 μm in the longitudinal direction. The computation accuracy was confirmed by decreasing the mesh size near the water-octane interface to 2.5 μm.

Fig. 11 shows how contact angles on the microchannel walls affected the two-phase flow patterns by the simulation. To unify the expressions of contact angle for the water and octane phases, hereafter, the contact angle is counted from the water phase to the octane phase. As described in the experimental section, the microchannel was placed horizontally, with upper hydrophilic and lower hydrophobic sections. Water and octane were introduced into the upper and lower inlets, respectively, at $v_{w,in} = v_{o,in} = 1$ cm s^{-1} in the calculation, as a representative case of the experiments. The broken line in the figure indicates a rough boundary for stability of the two-phase layered flow. The upper-left direction of Fig. 11 means that the upper section is more wettable to water, and that the lower section has a greater affinity for octane. The contact angles determined experimentally for the modified surfaces were greater than 175 degrees (5 degrees when defined as the angle of the water wedge) on the upper channel walls, and less than 7 degrees on the lower channel walls. The contact angles determined experimentally for the as-received PMMA plate were in the circled region near the boundary line. These suggest that the surface modification developed in the present study would effectively produce a water-octane layered flow. For the contact angles shown in the lower-right region of Fig. 11, the water-octane flow was fundamentally in the domain of a slug flow, and the mixture of water and octane was discharged with no separation.

Fig. 12 shows the effect of pressure applied to the lower outlet (octane side) of the microchannel. The contact angle of the water on the upper channel walls was assumed to be 165 degrees (15 degrees when defined as the angle of the water wedge), and that of octane on the lower channel walls was assumed to be 35 degrees. Under these conditions, the interface between water and octane was fixed along the boundary between the hydrophilic and hydrophobic sections. With no outlet pressure application, the water layer was convex downward because of the heavier density of water, as shown in Fig. 12(a). When pressure was applied to the lower outlet, on the other hand, the water layer was concave upward, as shown in Fig. 12(b). Both the simulation and experimental results suggest that the two-phase layered flow was maintained in the zone-selectively modified microchannels, even when pressure was unevenly applied to the outlet.

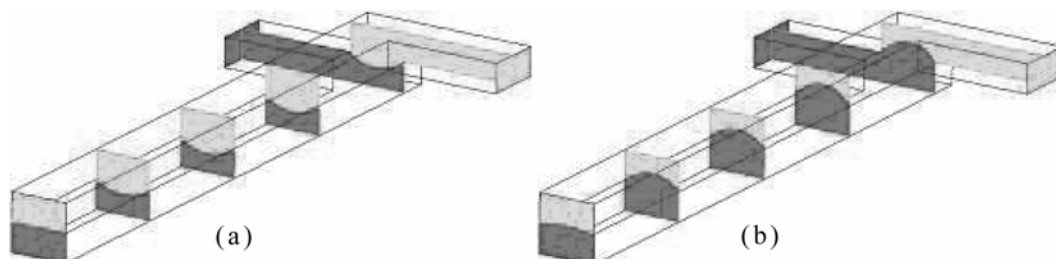CFD simulation, which was performed assuming no interfacial

Fig. 12. Effect of hydrostatic pressure applied to the upper side outlet: (a) applied pressure=0 Pa, (b) applied pressure=1.6 kPa.

tension, showed that the two-phase flow turned into a slug flow immediately after the water and octane flows merged. Thus, the interfacial tension is also important for the maintenance of a two-phase layered flow.

CONCLUSIONS

Microchannels 200 µm in width and 200 µm in depth were fabricated on PMMA plates for the purpose of contacting two immiscible liquids (water and octane). The upper and lower walls of the microchannels were modified to be hydrophilic and hydrophobic, respectively. A stable two-phase layered flow of water (upper phase) and octane (lower phase) was performed, and these liquids were virtually completely separated at a T-shaped bifurcate, under a range of flow rates tested. Both hydrophilicity and hydrophobicity of the modified surfaces were confirmed by a laser interference fringe technique. CFD simulation indicated that the contact angles, which were experimentally observed for the modified surfaces, were sufficient to maintain a stable water-octane layered flow.

ACKNOWLEDGMENTS

NOMENCLATURE

g (**g**) : gravitational acceleration (vector)
h   : height of liquid layer
Δh : incremental height difference of liquid layer between adjacent intensity extrema
i   : incident angle
ΔL : level of the outlet mouth elevated above microchannel
n_r : index of refraction
$\mathbf{n}_i$: unit vector normal to liquid-liquid contact plane
p_w, p_o : pressures of water and octane, respectively
$p_{u, out}$, $p_{l, out}$: pressures at upper- and lower-side outlets, respectively
Δp_{wo} : pressure difference across water and octane interface
t   : time
$v_{w, in}$, $v_{o, in}$: velocities at the inlet for water and octane, respectively
$\mathbf{v}_w$, $\mathbf{v}_o$: velocities (vector) of water and octane, respectively

Δx : distance between adjacent fringe stripes

Greek Letters
α : contact angle
γ : interfacial tension
λ : wave length of laser
μ_w, μ_o : viscosities of water and octane, respectively
ρ_w, ρ_o : densities of water and octane, respectively

REFERENCES

1. J. Choe, Y. Kwon, Y. Kim, H. S. Song and K. H. Song, *Korean J. Chem. Eng.*, **20**, 268 (2003).
2. V. Hessel, S. Hardt and H. Löwe, *Chemical micro process engineering, fundamentals, modelling and reactors*, Wiley-VCH Wiley-VCH, Weinheim, Germany (2003).
3. V. Hessel, H. Löwe, A. Müller and C. Kolb, *Chemical micro process engineering, processing and plants*, Wiley-VCH, Weinheim, Germany (2004).
4. K. I. Sotowa, R. Miyoshi, C. G. Lee, Y. Kang and K. Kusakabe, *Korean J. Chem. Eng.*, **22**, 552 (2005).
5. N. Kitamura, K. Ueno and H.-B. Kim, *Anal. Sic.*, **24**, 701 (2008).
6. J.-I .Yoshida, FLASH CHEMISTRY, *Fast organic synthesis in microsystems*, Wiley, Chichester, UK (2008).
7. V. Hessel, A. Renken, J. C. Shouten and J. Yoshida (edts.), *Micro process engineering, a comprehensive handbook*, Wiley-VCH, Weinheim, Germany (2009).
8. A.-L. Dessimos, L. Cavin, A. Renken and L. Kiwi-Minste, *Chem. Eng. Sci.*, **63**, 4035 (2008).
9. Y. Yamaguchi, F. Takagi, K. Yamashita, H. Nakamura and H. Maeda, *AIChE J.*, **50**, 1530 (2004).
10. Y. Yamaguchi, T. Honda, M. P. Briones, K. Yamashita, M. Miyazaki, H. Nakamura and H. Maeda, *Chem. Eng. Technol.*, **30**, 379 (2007).
11. B. Zhao, N. O. L. Viernes, J. S. Moore and D. J. Beebe, *J. Am. Chem. Soc.*, **124**, 5284 (2002).
12. H.-B. Kim, K. Ueno, M. Chiba, O. Kogi and N. Kitamura, *Anal. Sci.*, **16**, 871 (2000).
13. A. Hibara, M. Tokeshi, K. Uchiyama, H. Hisamoto and T. Kitamori, *Anal. Sci.*, **17**, 89 (2001).
14. A. Hibara, M. Nonaka, H. Hisamoto, K. Uchiyama, Y. Kikutani, M. Tokeshi and T. Kitamori, *Anal. Chem.*, **74**, 1724 (2002).
15. A. Arata, A. Hibara and T. Kitamori, *Anal. Chem.*, **79**, 3919 (2007).
16. A. Kariyasaki, Y. Yamasaki, M. Kagawa, T. Nagashima, A. Ousaka and S. Morooka, *Heat Transfer Eng.*, **30**, 28 (2009).
17. Y. Yamasaki, M. Goto, A. Kariyasaki and S. Morooka, *Kagaku Kogaku Ronbunshu*, **34**, 175 (2008).